Supporting Information File

Quantitative Raman microscopy to describe structural organisation in hollow microcrystals built from silicon catecholate and amines

*Victor V. Volkov,[a] Toby J Blundell,[b] Stephen Argent,[c] Carole C. Perry[a]**

[a]Interdisciplinary Biomedical Research Centre, School of Science and Technology, Nottingham Trent University, Clifton Lane, Nottingham NG11 8NS, United Kingdom.
[b]Department of Chemistry and Forensics, School of Science and Technology, Nottingham Trent University, Clifton Lane, Nottingham NG11 8NS, United Kingdom.
[c]School of Chemistry, University of Nottingham, University Park, Nottingham NG7 2RD.

Crystal Structure Data

Table S1. Crystal Data for TCS-TEMED

Compound	**TCS-TEMED**
Formula	$C_{24}H_{30}N_2O_6Si$
$D_{calc.}$/ g cm^{-3}	1.399
μ/mm^{-1}	0.140
Formula Weight	470.59
Colour	clear colourless
Shape	needle-shaped
Size/mm^3	0.15×0.01×0.01
T/K	100.15
Crystal System	monoclinic
Space Group	$C2/c$
a/Å	12.3695(2)
b/Å	21.4394(3)
c/Å	8.54050(10)
α/°	90
β/°	99.4420(10)
γ/°	90
V/Å^3	2234.21(5)
Z	4
Z'	0.5
Wavelength/Å	0.6889
Radiation type	Synchrotron
Θ_{min}/°	2.981
Θ_{max}/°	27.336
Measured Refl's.	2782
Indep't Refl's	2782
Refl's I≥2 σ(I)	2532
R_{int}	.
Parameters	191
Restraints	326
Largest Peak	0.652
Deepest Hole	-0.614
GooF	1.154
wR_2 (all data)	0.2467
wR_2	0.2435
R_1 (all data)	0.0834
R_1	0.0792

Experimental. Single clear colourless needle-shaped crystals of **TCS-TEMED** were used as supplied. A suitable crystal with dimensions 0.15 × 0.01 × 0.01 mm^3 was selected and mounted on a MITIGEN holder in perfluoroether oil on a Fluid Film Devices diffractometer. The crystal was kept at a steady T = 100.15 K during data collection. The structure was solved with the **ShelXT** [S1] solution program using dual methods and by using **Olex2** 1.5-beta [S2] as the graphical interface. The model was refined with **ShelXL** 2018/3 [S3] using full matrix least squares minimisation on $\boldsymbol{F^2}$.

Crystal Data. $C_{24}H_{30}N_2O_6Si$, M_r = 470.59, monoclinic, $C2/c$ (No. 15), a = 12.3695(2) Å, b = 21.4394(3) Å, c = 8.54050(10) Å, β = 99.4420(10)°, α = γ = 90°, V = 2234.21(5) $Å^3$, T = 100.15 K, Z = 4, Z' = 0.5, μ(Synchrotron) = 0.140, 2782 reflections measured, 2782 unique (R_{int} = .) which were used in all calculations. The final wR_2 was 0.2467 (all data) and R_1 was 0.0792 (I≥2 σ(I)).

Data were measured using ϕ and ω rotation with 0.1 degree frames with Synchrotron radiation. The diffraction pattern was indexed and the total number of runs and images was based on the strategy calculation from the program GDA 8.44; generic data acquisition software. The maximum resolution that was achieved was Θ = 27.336° (0.75 Å).

The unit cell was refined using aimless [S4] ccp4 [S5] DIALS 2.1.1-gcdd629a7b-release [S6] pointless [S7] XIA2 0.6.366-ga657f9d9-dials-2.1 [S8] on 8899 reflections.

Data reduction, scaling and absorption corrections were performed using aimless [S4] ccp4 [S5] DIALS 2.1.1-gcdd629a7b-release [S6] pointless [S7] XIA2 0.6.366-ga657f9d9-dials-2.1 [S8]. The final completeness is 99.60 % out to 27.336° in Θ. An empirical absorption correction was performed using CCP4 7.0.078: AIMLESS, version 0.7.4 : 13/12/18 Scaling & analysis of unmerged intensities, absorption correction using spherical harmonics. The absorption coefficient μ of this material is 0.140 mm^{-1} at this wavelength (λ = 0.68890Å) and the minimum and maximum transmissions are 0.997 and 1.000.

The structure was solved using Olex2 [S2] and the space group $C2/c$ (# 15) determined by the ShelXT [S1] structure solution program using dual methods and refined by full matrix least squares minimisation on $\boldsymbol{F^2}$ using version 2018/3 of **ShelXL** [S3]. All non-hydrogen atoms were refined anisotropically. Heteroatom hydrogens were located from the difference map, all other hydrogen positions were calculated geometrically and refined using the riding model.

_refine_special_details: Diamine disordered across special position - modelled in part -1 at half occupancy. Twin Law 0.511 0.489 0.359 1.511 -0.511 0.359 0 0 -1 (2-axis 1 1 0 3 1 1 Angle = 3.38 Deg).

_exptl_absorpt_process_details: CCP4 7.0.078: AIMLESS, version 0.7.4 : 13/12/18 Scaling & analysis of unmerged intensities, absorption correction using spherical harmonics.

The value of Z' is 0.5. This means that only half of the formula unit is present in the asymmetric unit, with the other half consisting of symmetry equivalent atoms. Tetramethylethylenediamine (TEMED) was disordered across a special position and was modelled as a whole molecule in part -1.

Reflection Statistics

Total reflections (after filtering)	3243	Unique reflections	2782
Completeness	0.998	Mean I/σ	11.03
hkl_{max} collected	(20, 36, 14)	hkl_{min} collected	(-20, -36, -14)
hkl_{max} used	(16, 28, 11)	hkl_{min} used	(-16, 0, 0)
Lim d_{max} collected	100.0	Lim d_{min} collected	0.75
d_{max} used	6.62	d_{min} used	0.75
Friedel pairs	634	Friedel pairs merged	1
Inconsistent equivalents	0	R_{int}	-1.0
R_{sigma}	0.1013	Intensity transformed	0
Omitted reflections	0	Omitted by user (OMIT hkl)	0
Multiplicity	(6103, 81)	Maximum multiplicity	3
Removed systematic absences	0	Filtered off (Shel/OMIT)	3020

Table S2: Fractional Atomic Coordinates ($\times 10^4$) and Equivalent Isotropic Displacement Parameters ($Å^2 \times 10^3$) for **TCS-TEMED**. U_{eq} is defined as 1/3 of the trace of the orthogonalised U_{ij}.

Atom	x	y	z	U_{eq}
Si1	5000	3423.2(6)	7500	13.4(3)
O1	4860(2)	3984.7(11)	8980(3)	15.5(5)
O2	3557(2)	3433.6(12)	6888(3)	16.9(5)
O3	5076(2)	2815.0(11)	6056(3)	17.0(5)
C1	3815(3)	4174.9(15)	8880(4)	14.3(6)
C2	3071(3)	3858.7(16)	7719(4)	15.6(6)
C3	1960(3)	3991.4(18)	7524(4)	20.8(7)
C4	1593(3)	4444.8(19)	8488(5)	23.4(8)
C5	2321(3)	4762.1(17)	9617(5)	22.7(8)
C6	3447(3)	4634.6(16)	9818(4)	19.1(7)
C7	5052(3)	2238.0(15)	6693(4)	14.1(6)
C8	5137(3)	1682.5(16)	5898(4)	16.9(7)
C9	5073(3)	1119.7(17)	6709(5)	20.5(7)
N1	3640(20)	3198(13)	3410(40)	14(3)
N2	6290(20)	3270(13)	1750(40)	13(3)
C10	4358(5)	3083(3)	2224(8)	16.7(13)
C11	2770(7)	2719(4)	3333(10)	25.2(16)
C12	3076(19)	3851(9)	3140(30)	25(4)
C13	5362(5)	3502(3)	2504(8)	14.7(12)
C14	6784(7)	2692(4)	2602(11)	30.2(18)
C15	7097(18)	3746(9)	1650(30)	20(3)

Table S3: Anisotropic Displacement Parameters (×10^4) for **TCS-TEMED**. The anisotropic displacement factor exponent takes the form: $-2\pi^2[h^2a^{*2} \times U_{11} + ... + 2hka^* \times b^* \times U_{12}]$

Atom	U_{11}	U_{22}	U_{33}	U_{23}	U_{13}	U_{12}
Si1	20.9(6)	11.3(6)	7.8(6)	0	2.0(5)	0
O1	19.9(12)	12.5(11)	13.9(11)	-4.8(9)	2.1(9)	-0.2(9)
O2	21.6(12)	17.1(12)	11.4(11)	-3.8(9)	1.4(9)	-3.6(9)
O3	29.3(13)	11.8(11)	9.8(11)	-1.1(9)	2.7(9)	1.4(9)
C1	21.0(15)	11.7(14)	10.5(14)	1.3(11)	3.6(11)	-0.3(12)
C2	21.9(16)	14.3(15)	10.9(14)	3.1(11)	3.4(12)	-0.4(12)
C3	20.0(16)	21.6(17)	20.6(17)	4.4(14)	2.4(13)	-1.8(13)
C4	21.5(17)	23.2(18)	26.8(18)	5.6(14)	7.8(14)	3.6(14)
C5	32.0(19)	16.5(16)	21.8(17)	2.3(13)	10.3(15)	5.6(14)
C6	28.3(17)	13.1(15)	16.6(16)	-0.2(12)	5.6(13)	-1.0(13)
C7	16.3(15)	12.8(14)	13.0(16)	-0.2(12)	1.4(11)	0.5(11)
C8	18.4(16)	14.8(15)	17.8(16)	-2.8(12)	3.6(12)	-0.1(12)
C9	21.5(17)	13.0(15)	27.2(19)	-2.2(13)	4.6(14)	0.4(12)
N1	17(4)	15(6)	11(6)	4(4)	6(3)	0(3)
N2	17(5)	13(5)	8(6)	-2(4)	0(4)	4(3)
C10	17(3)	19(3)	15(3)	-7(2)	5(2)	-4(2)
C11	23(3)	25(4)	29(4)	-4(3)	8(3)	-8(3)
C12	32(8)	19(6)	25(8)	7(5)	13(5)	10(5)
C13	16(2)	19(3)	9(3)	-6(2)	3(2)	3(2)
C14	27(4)	25(4)	38(5)	7(3)	4(4)	10(3)
C15	24(6)	24(6)	13(6)	-5(5)	6(4)	-5(5)

Table S4: Bond Lengths in Å for **TCS-TEMED**.

Atom	Atom	Length/Å
Si1	O1[1]	1.774(2)
Si1	O1	1.774(2)
Si1	O2[1]	1.776(3)
Si1	O2	1.776(3)
Si1	O3[1]	1.808(3)
Si1	O3	1.808(3)
O1	C1	1.345(4)
O2	C2	1.355(4)
O3	C7	1.354(4)
C1	C2	1.411(5)
C1	C6	1.393(5)
C2	C3	1.386(5)
C3	C4	1.396(5)
C4	C5	1.385(6)
C5	C6	1.402(5)
C7	C7[1]	1.406(6)
C7	C8	1.383(5)
C8	C9	1.400(5)
C9	C9[1]	1.393(8)
N1	C10	1.48(3)
N1	C11	1.48(2)
N1	C12	1.56(4)
N2	C13	1.50(2)
N2	C14	1.51(3)
N2	C15	1.44(4)
C10	C13	1.519(9)

––––

[1]1-x,+y,3/2-z

Table S5: Bond Angles in ° for **TCS-TEMED**.

Atom	Atom	Atom	Angle/°
O1[1]	Si1	O1	94.54(17)
O1	Si1	O2	89.44(11)
O1	Si1	O2[1]	89.58(12)
O1[1]	Si1	O2	89.58(12)
O1[1]	Si1	O2[1]	89.44(11)
O1[1]	Si1	O3[1]	175.85(12)
O1[1]	Si1	O3	88.95(11)
O1	Si1	O3[1]	88.95(11)
O1	Si1	O3	175.84(12)
O2	Si1	O2[1]	178.55(18)
O2[1]	Si1	O3	92.72(12)
O2[1]	Si1	O3[1]	88.33(12)
O2	Si1	O3[1]	92.72(12)
O2	Si1	O3	88.32(12)
O3[1]	Si1	O3	87.66(16)
C1	O1	Si1	111.5(2)
C2	O2	Si1	111.4(2)
C7	O3	Si1	112.2(2)
O1	C1	C2	114.1(3)
O1	C1	C6	125.4(3)
C6	C1	C2	120.4(3)
O2	C2	C1	113.4(3)
O2	C2	C3	126.3(3)
C3	C2	C1	120.4(3)
C2	C3	C4	118.9(4)
C5	C4	C3	121.0(4)
C4	C5	C6	120.6(3)
C1	C6	C5	118.6(3)

Atom	Atom	Atom	Angle/°
O3	C7	C7[1]	113.92(17)
O3	C7	C8	125.5(3)
C8	C7	C7[1]	120.5(2)
C7	C8	C9	119.0(3)
C9[1]	C9	C8	120.5(2)
C10	N1	C11	112(2)
C10	N1	C12	110.6(18)
C11	N1	C12	108(2)
C13	N2	C14	110.0(18)
C15	N2	C13	112.2(18)
C15	N2	C14	113(2)
N1	C10	C13	111.3(12)
N2	C13	C10	113.8(13)

––––
[1]1-x,+y,3/2-z

Table S6: Torsion Angles in ° for **TCS-TEMED**.

Atom	Atom	Atom	Atom	Angle/°
Si1	O1	C1	C2	4.2(3)
Si1	O1	C1	C6	-176.6(3)
Si1	O2	C2	C1	-1.5(3)
Si1	O2	C2	C3	179.0(3)
Si1	O3	C7	C7[1]	1.4(5)
Si1	O3	C7	C8	-177.5(3)
O1[1]	Si1	O1	C1	85.4(2)
O1[1]	Si1	O2	C2	-91.4(2)
O1	Si1	O2	C2	3.1(2)
O1[1]	Si1	O3	C7	177.1(2)
O1	C1	C2	O2	-1.8(4)
O1	C1	C2	C3	177.7(3)
O1	C1	C6	C5	-177.3(3)
O2[1]	Si1	O1	C1	174.8(2)
O2	Si1	O1	C1	-4.1(2)
O2[1]	Si1	O3	C7	87.7(2)
O2	Si1	O3	C7	-93.3(2)
O2	C2	C3	C4	179.9(3)
O3[1]	Si1	O1	C1	-96.9(2)
O3[1]	Si1	O2	C2	92.1(2)
O3	Si1	O2	C2	179.6(2)
O3[1]	Si1	O3	C7	-0.51(17)
O3	C7	C8	C9	-178.6(3)
C1	C2	C3	C4	0.4(5)
C2	C1	C6	C5	1.9(5)
C2	C3	C4	C5	0.4(6)
C3	C4	C5	C6	0.0(6)
C4	C5	C6	C1	-1.2(5)
C6	C1	C2	O2	178.9(3)
C6	C1	C2	C3	-1.5(5)
C7[1]	C7	C8	C9	2.6(6)
C7	C8	C9	C9[1]	-0.1(6)
N1	C10	C13	N2	160(2)
C11	N1	C10	C13	-169.7(16)
C12	N1	C10	C13	70(2)
C14	N2	C13	C10	-70(2)
C15	N2	C13	C10	163.8(18)

––––
[1]1-x,+y,3/2-z

Table S7: Hydrogen Fractional Atomic Coordinates (×10^4) and Equivalent Isotropic Displacement Parameters (Å^2×10^3) for **TCS-TEMED**. U_{eq} is defined as 1/3 of the trace of the orthogonalised U_{ij}.

Atom	x	y	z	U_{eq}
H3	1456.77	3777.45	6747.83	25
H4	833.05	4536.91	8366.15	28
H5	2054.12	5068.73	10260.63	27
H6	3948.18	4857.22	10579.11	23

Atom	x	y	z	U_{eq}
H8	5237.32	1683	4818.79	20
H9	5129.02	735.08	6175.4	25
H1	4090.93	3188.71	4496.77	17
H2	5985.72	3144.11	640.47	16
H10A	3944.34	3160.69	1148.12	20
H10B	4593.87	2641.32	2280.62	20
H11A	2260.61	2832.83	4051.03	38
H11B	3103.81	2313.77	3649.64	38
H11C	2371.79	2691.86	2244.22	38
H12A	3638.99	4177.17	3262	37
H12B	2590.77	3915.84	3928.35	37
H12C	2647.42	3869.66	2073.34	37
H13A	5151.4	3922.79	2082.51	18
H13B	5611.34	3542.73	3661.93	18
H14A	6201.33	2387.9	2669.53	45
H14B	7143.54	2803.67	3674.27	45
H14C	7322.98	2509.41	2014.02	45
H15A	6751.87	4095.3	1019.57	31
H15B	7689.44	3574.65	1149.31	31
H15C	7397.03	3892.59	2722.9	31

Table S8: Atomic Occupancies for all atoms that are not fully occupied in **TCS-TEMED**.

Atom	Occupancy
N1	0.5
H1	0.5
N2	0.5
H2	0.5
C10	0.5
H10A	0.5
H10B	0.5
C11	0.5
H11A	0.5
H11B	0.5
H11C	0.5
C12	0.5
H12A	0.5
H12B	0.5
H12C	0.5
C13	0.5
H13A	0.5
H13B	0.5
C14	0.5
H14A	0.5
H14B	0.5
H14C	0.5
C15	0.5
H15A	0.5
H15B	0.5
H15C	0.5

Table S9. Hydrogen bonds with H..Acceptor < r(A) + 2.000 Å and DHA angle > 110°.

Donor-H	Donor-H distance/ Å	H..Acceptor distance/ Å	DHA Angle/ °	Donor..Acceptor distance/ Å	Acceptor [symmetry operation]
N(1)-H(1)	1	2.367	132.71	3.15(3)	O1 [-x+1, y, -z+3/2]
N(1)-H(1)	1	2.278	128.95	3.03(3)	O2
N(1)-H(1)	1	1.870	150.04	2.76(4)	O3
N(2)-H(2)	1	2.591	114.26	3.12(3)	O1 [x, y, z-1]
N(2)-H(2)	1	2.436	130.71	3.16(3)	O2 [-x+1, y, -z+1/2]
N(2)-H(2)	1	1.899	158.62	2.87(3)	O3 [-x+1, y, -z+1/2]
C(10)-H(10A)	0.990	2.497	115.05	3.052(7)	O3 [-x+1, y, -z+1/2]
C(13)-H(13A)	0.990	2.606	114.63	3.147(7)	O1 [x, y, z-1]
C(13)-H(13B)	0.990	2.381	143.59	3.230(7)	O1 [-x+1, y, -z+3/2]
C(14)-H(14C)	0.980	2.558	141.39	3.383(9)	O2 [x+1/2, -y+1/2, z-1/2]

Citations

[S1] G. M. Sheldrick, *Acta Cryst.*, (2015), **A71**, 3-8.

[S2] O.V. Dolomanov, L.J. Bourhis, R.J. Gildea, J.A.K. Howard and H. Puschmann, *J. Appl. Cryst.*, (2009), **42**, 339-341.

[S3] G. M. Sheldrick, *Acta Cryst.*, (2015), **C71**, 3-8.

[S4] P. R. Evans and G. N. Murshudov, *Acta Cryst.* (2013), **D69**, 1204-1214.

[S5] M. D. Winn, C. C. Ballard, K. D. Cowtan, E. J. Dodson, P. Emsley, P. R. Evans, R. M. Keegan, E. B. Krissinel, A. G. W. Leslie, A. McCoy, S. J. McNicholas, G. N. Murshudov, N. S. Pannu, E. A. Potterton, H. R. Powell, R. J. Read, A. Vagin and K. S. Wilson, *Acta Cryst.*, (2011), **D67**, 235-242.

[S6] G. Winter, D. G. Waterman, J. M. Parkhurst, A. S. Brewster, R. J. Gildea, M. Gerstel, L. Fuentes-Montero, M. Vollmar, T. Michels-Clark, I. D. Young, N. K. Sauter and G. Evans. *Acta Cryst.*, (2018), **D74**, 85-97.

[S7] P. Evans, *Acta Cryst.*, (2006), **D62**, 72-82.

[S8] G.J. Winter*, Appl. Cryst.*, (2010). **43**, 186-190.

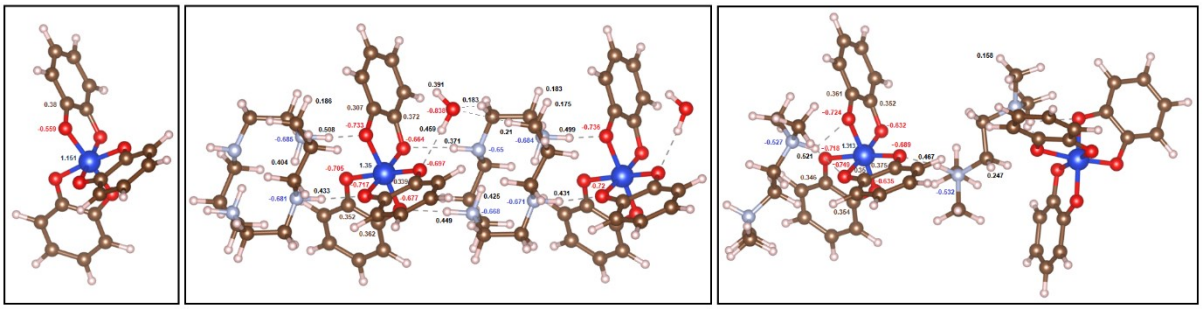

Chart S1. *Mulliken charges computed for tris(1,2-benzenediolato-O,O')silicate alone and selected segments of the structural units of TCS-CYCLAM and TCS-TEMED embedded in a crystalline environment as we describe in the Materials and Methods of the main text.*

Spectroscopy

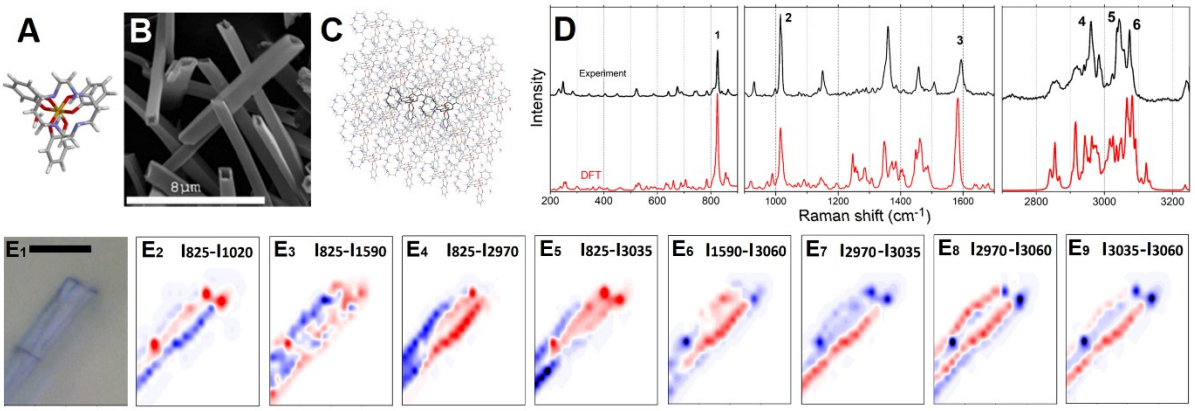

Figure S1. A: *TCS-CYCLAM molecular structure from X-ray diffraction,* ***B:*** *SEM of TCS- CYCLAM typical microcrystals, scale bar = 8 um;* ***C:*** *graphical representation for the two-layer ONIOM crystalline clusters; thin grey lines and thicker black lines show the structural units treated at classical and quantum levels respectively;* ***D:*** *Comparison of experimentation-polarized Raman response with ONIOM DFT analysis for TCS-CYCLAM in the low, middle and high frequency range. Indices at experimental resonances indicate spectral modes used for Raman microscopy imaging;* ***E1:*** *light microscope image (collected on crystals used for Raman microscopy) of hollow TCS-CYCLAM microcrystal, scale bar = 10 micron.* ***E2-E9****, differences of normalised Raman microscopy images reconstructed at Raman wavenumbers, as indicate.*

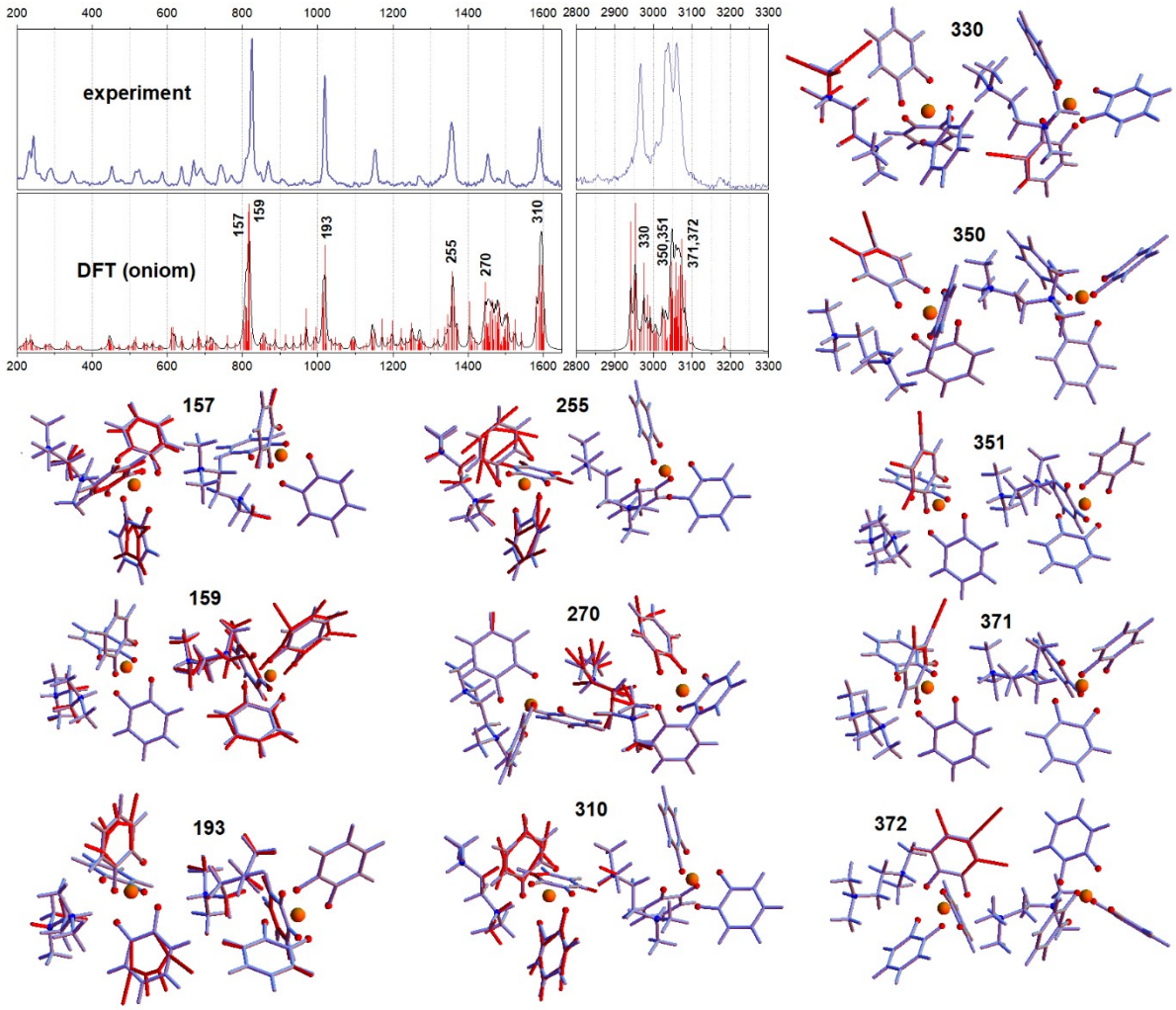

Figure S2. *Experimental and computed isotropic Raman spectra and graphic visualisation of the main normal modes according to predictions of DFT for TCS-TEMED microcrystals*

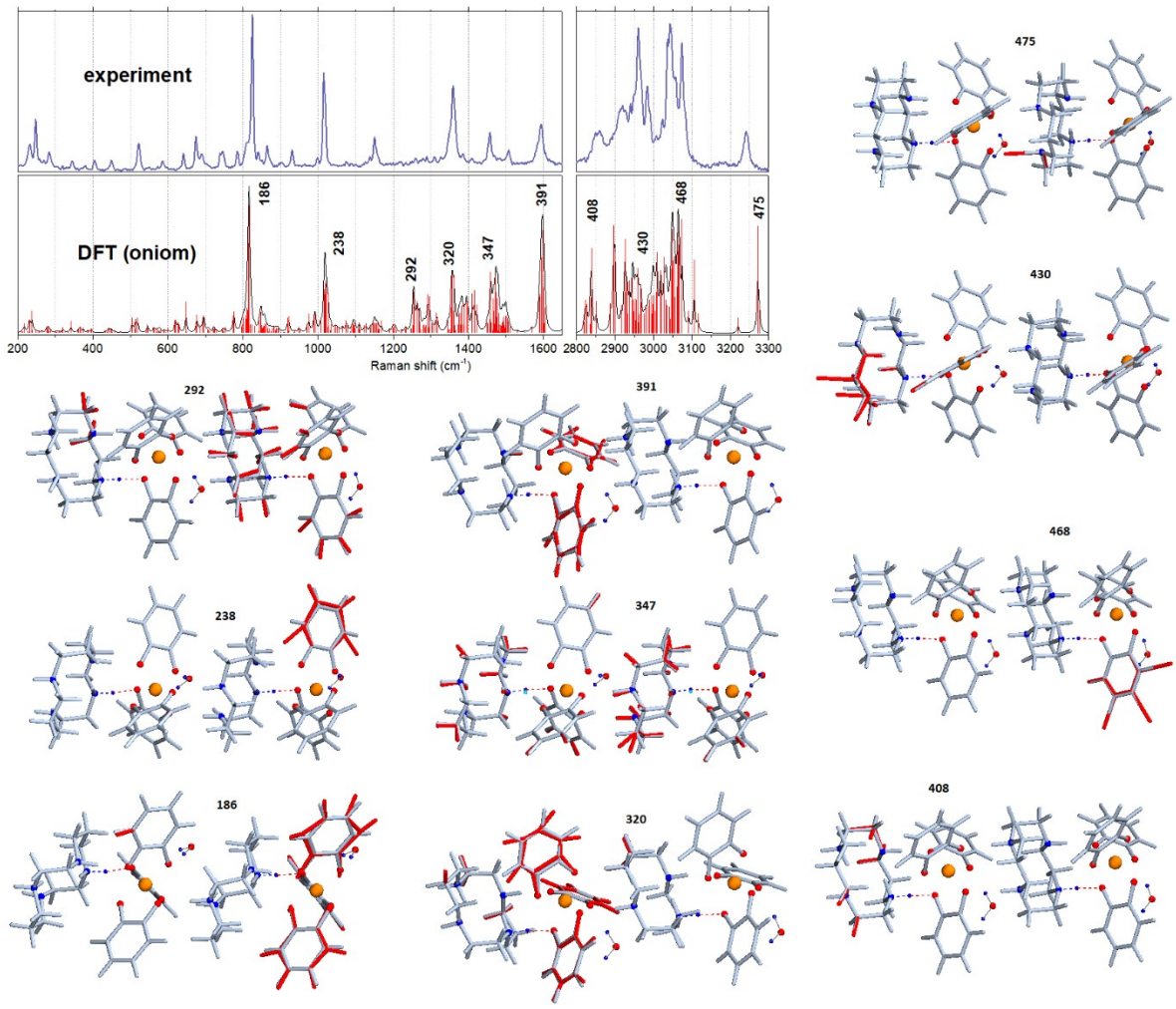

Figure S3. *Experimental and computed isotropic Raman spectra and graphic visualisation of the main normal modes according to predictions of DFT for TCS-CYCLAM microcrystals.*

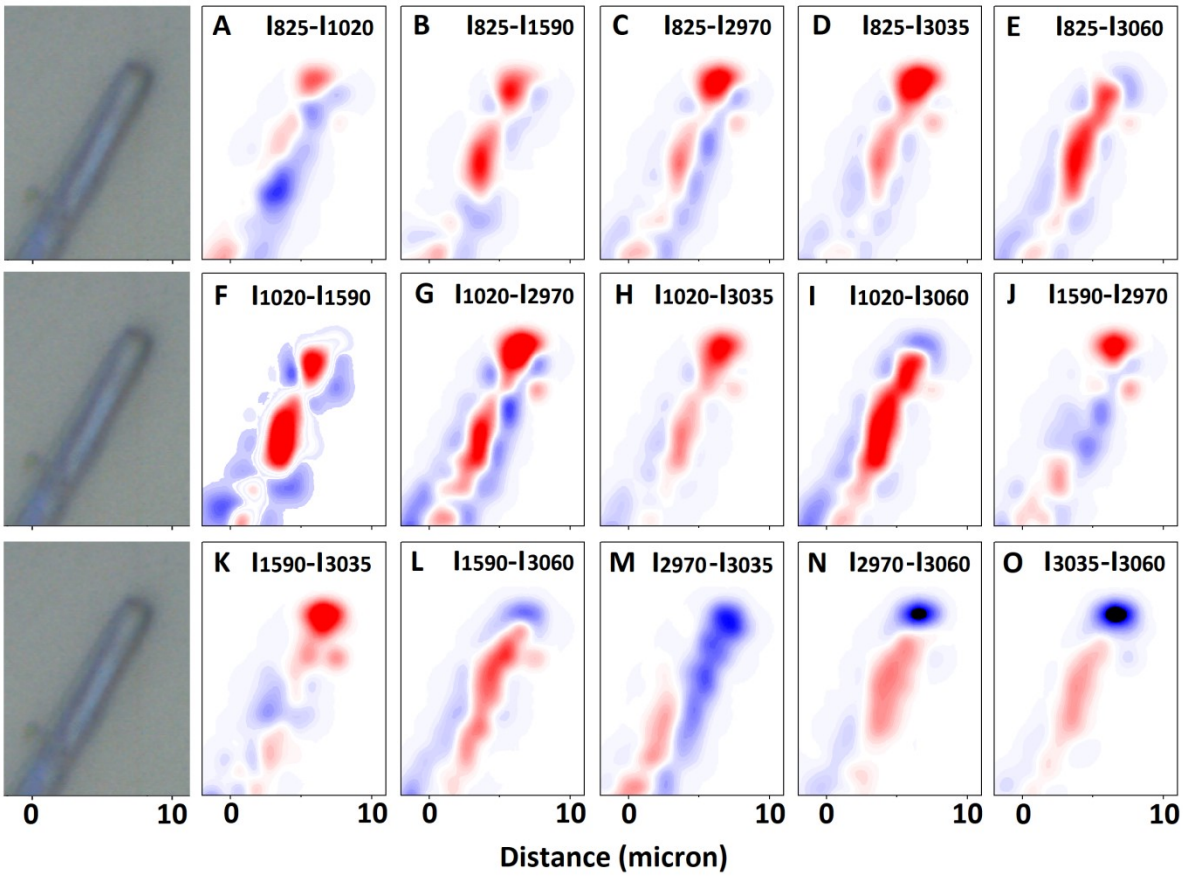

***Figure S4**. Raman microscopy studies of the TCS-TEMED microcrystal. Differences of normalised Raman microscopy images Im_i-Im_j reconstructed at Raman wavenumbers, as indicated.*

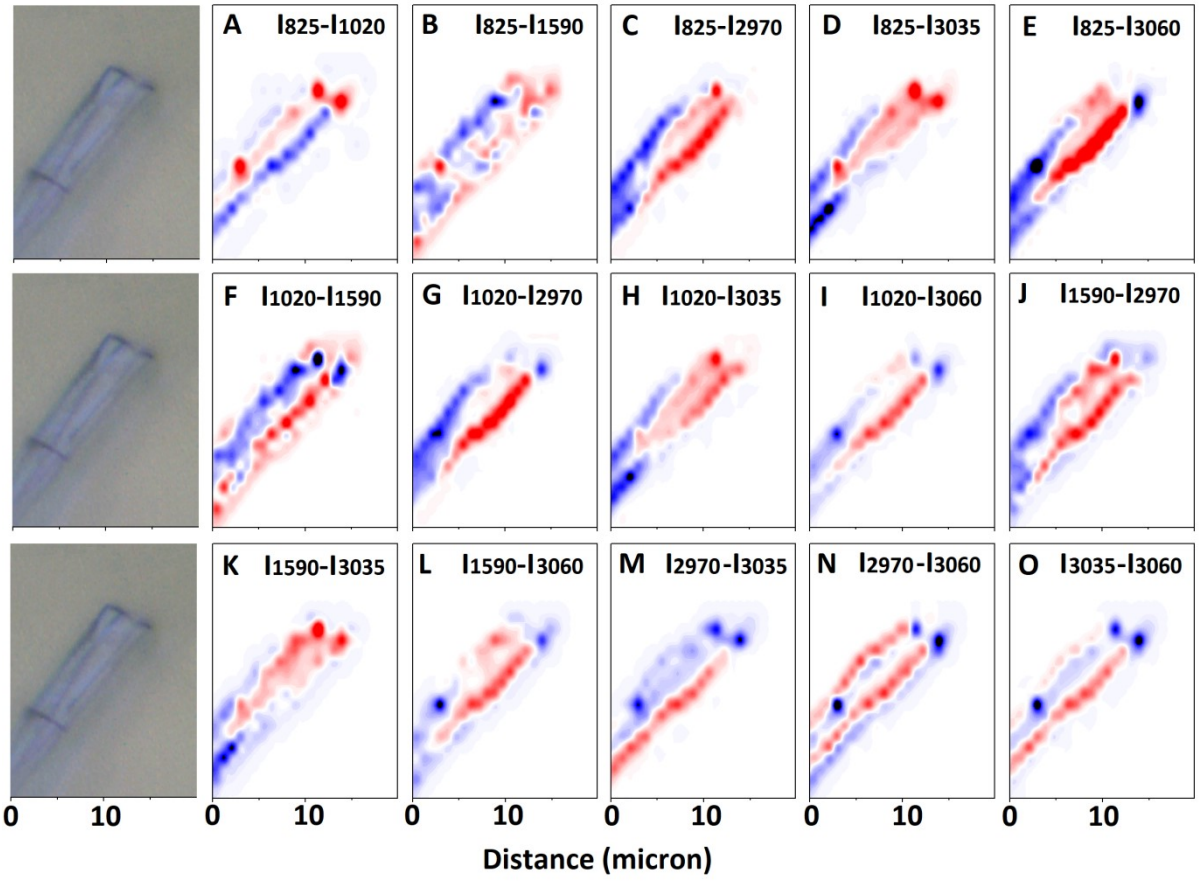

Figure S5. *Raman microscopy studies of the TCS-CYCLAM microcrystal. Differences of normalised Raman microscopy images Im_i-Im_j reconstructed at Raman wavenumbers, as indicated*.

To account structural variances, we took 9 acquisitions of polarization specific Raman spectra: we sample three TCS-TEMED microcrystals at three different spots. Each acquisition (taken at the same spot) consists of two spectra: one spectrum is for polarization planes of the exciting and of the sampled field are along the long axis of a microcrystal (II); another spectrum is when polarization planes of the exciting and of the sampled fields are across the long axis of a microcrystal (⊥). Taking a number of acquisitions is important because we attempt to characterise not a single crystal but polycrystalline assemblies: after all we wish to characterise structural tendencies in assemblies of complex nature.

To describe variance ranges, each pair of spectra is normalised by the intensity of Raman signal at 1021 cm^{-1} sampled under parallel setting. Accordingly, as one may see in Figure S6, the I_{II} intensity at 1021 cm^{-1} is equal to 1 and without a variance. In respect to this reference, the pink and the cyan colored regions (see Figure S6) describe the variance regions of Raman activities sampled at the indicated frequencies under parallel and perpendicular experimental geometries, respectively. Consistently, black and blue lines in Figure S6 are the mean intensities sampled under parallel and perpendicular geometries, respectively.

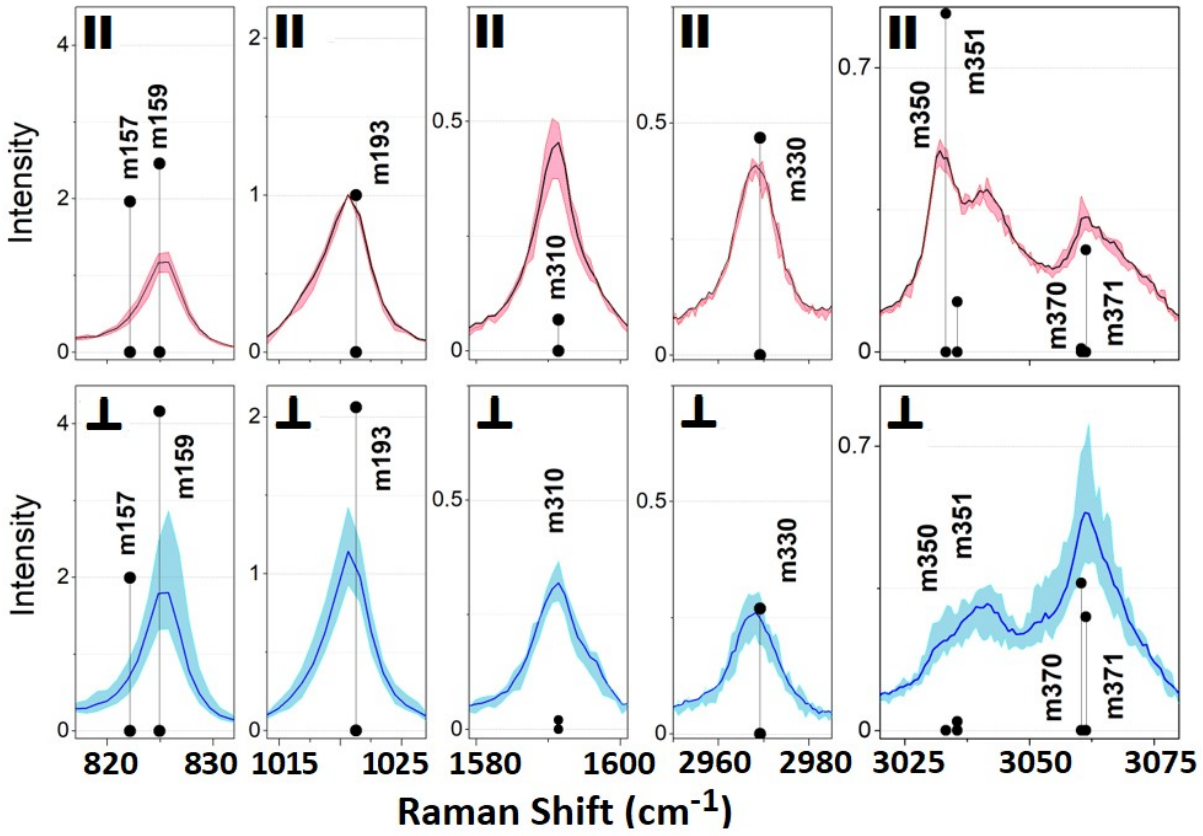

Figure S6. *polarization Raman activities in TCS-TEMED microcrystals normalised by the intensity of Raman scattering at 1021 cm^{-1} sampled under parallel setting. Pink and the cyan regions describe the variance regions of Raman activities sampled at the indicated frequencies under parallel and perpendicular experimental geometries, respectively. Black and blue lines are the mean intensities sampled under parallel and perpendicular geometries, respectively. Black circle-line intensities are computed responses to compare with the experimental data according to the structural search as described in the following text and in Figure S7.*

Using Eq. 2-4 in the main text, we compute I_{xx} and I_{yy} intensities in $\{\Psi, \Phi\}$ angular space when Θ varies from 0^o to 90^o to match best the tendencies for various experimental resonances. Here, it is important to notice that the strong difference of intensities under parallel and perpendicular polarisation for the Raman resonances at 3035 and 3060 cm^{-1} is particularly helpful. For example, in Figures S7A-S7D, we use color filled regions to indicate the $\{\Psi, \Phi\}$ angular regions for $\Theta = 60^o$, where the ratio I_{XX}/I_{YY} for the computed intensities at 825, 1020, 3035 and 3060 cm^{-1}, respectively, would be most proximal to the observed in experiment (to fall within the variance ranges by pink and cyan fields in Figure S6).

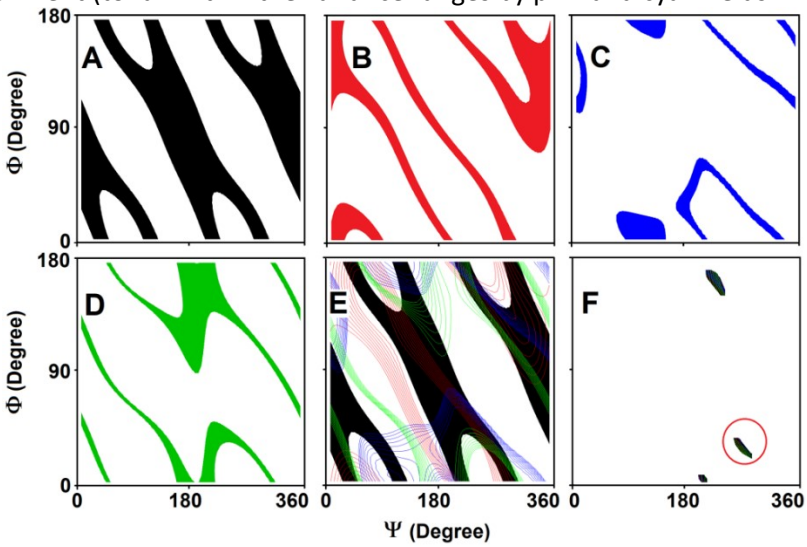

Figure S7. *Ratio of I_{xx}/I_{yy} intensities computed for the DFT predicted resonances at about 824 (**A**), 1021 (**B**), 3030 (**C**) and 3060 cm^{-1} (**D**) in dependence on the $\{\Psi, \Phi\}$ Euler angles when $\Theta = 60^o$. Solid colors indicate the orientation region where the ratio of intensity would fall in the acceptable ranges in the spectra at the left (by pink and cyan variation regions). **E** and **F:** overlap of the date shown in panels **A-D** and the regions of the overlap. Red circled region is the best match to provide the intensities as presented by black circle-line signals at the left.*

Next, in Figure S7E we overlap the angular maps, and in Figure S7F we show the angular regions to satisfy the four considered angular dependences. Finally, here, the circled region in Figure S6F suggests the best match to the variances observed experimentally: $\Theta = 60^o \pm 10^o$, $\Psi = 40^o \pm 10^o$, and $\Phi = 250^o \pm 10^o$. For this orientation, we use Eq. 2-4 as we present in the main text to compute solid circle intensities as shown in Figure S6.

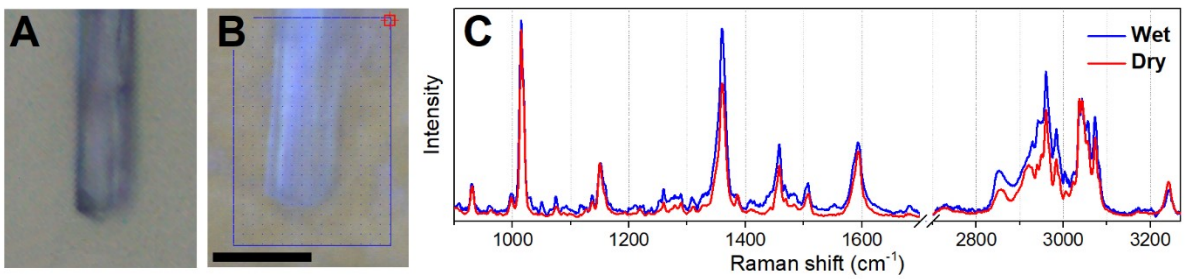

Figure S8. ***A:*** *Bright field image of dry TSC-CYCLAM crystal.* ***B:*** *Bright field image of the TSC-CYCLAM crystal after adding D_2O, scale bar = 10 micron. We observe swelling and change of optical properties, what suggests that water is absorbed by crystal walls.* ***C:*** *average Raman spectra of TSC-CYCLAM crystal before (red) and after adding D_2O (blue). Since we do not observe obvious Raman modes due to OD stretching and bending, this suggests that water distributes as isolated molecules, which are not Raman active. Some broadening and merging of peaks at 2950 cm^{-1} suggests restructuring.*

To explore possible effects of orientation in Raman microscopy, first, in Figure S9 A1-C1, we present difference images computed in the XY plane of the laboratory frame for the microcrystal with its long axis oriented along the Y axis of the laboratory frame. Specifically, we use the top slab selection coloured with magenta, see panel D1. The images in Figure S9 A1-B1 are identical to those presented in Figure 4 in the main text. Next, in Figure S9 A2-C2, we present images top slab selection coloured with blue, see panel D2, after the crystal was turned by 60° about its long axis (which is parallel to the Y axis of the laboratory frame). In result, we see that for the adopted orientation model (all unit cells are oriented the same) the computed images demonstrate that the difference patterns for the two crystals under different orientations have similar character. This we may not expect if a synthesized microcrystal would have polycrystalline domains.

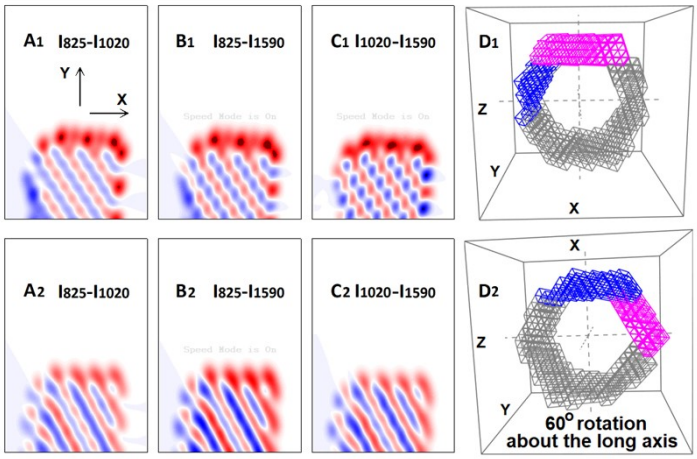

Figure S9. ***A₁-C₁:*** *modelling of XY plane Raman difference images using computed Raman responses for the top (magenta colour) region of a theoretical hexagonal hollow assembly,* ***D₁****, as in* ***Figure 4*** *in the main text.* ***A₂-C₂:*** *modelling of XY plane Raman difference images using computed Raman responses for the top (blue colour) region selected using the theoretical hexagonal hollow assembly rotated by 60° about the long axis,* ***D₂****.*

To demonstrate resolving power of the approach, in Figure S10 we present computed XZ plane Raman difference images. It is interesting to note that for the Raman resonances chosen, theory predicts two different orientations about the nodal line in Raman patterns (see black arrows). This reflects the special relative arrangement of the Raman active moieties in dependence on the unit cell packing. In the case of different orientation of the unit cells or presence of structural domains, one should expect a pattern complexity to stimulate further computational efforts assisted with machine learning with a promise to understand the present diversity in more detail.

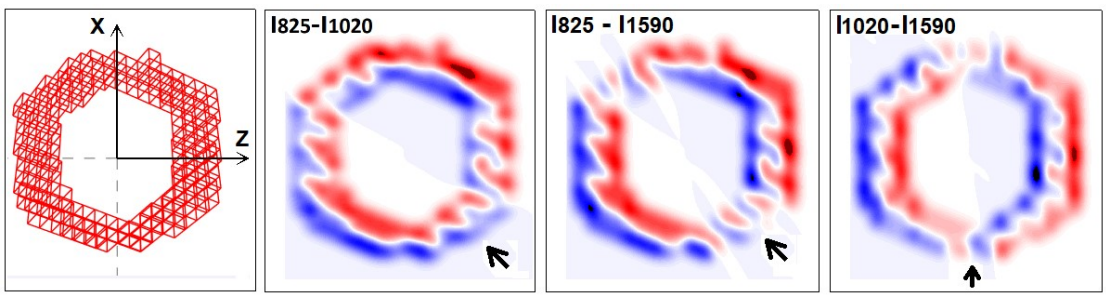

Figure S10. *Computed XZ plane Raman difference images of theoretical hexagonal hollow assembly, as shown in the left panel.*